Bioresource Technology 284 (2019) 139–147

Contents lists available at ScienceDirect

Bioresource Technology

journal homepage: www.elsevier.com/locate/biortech

Experimental and model enhancement of food waste hydrothermal liquefaction with combined effects of biochemical composition and reaction conditions

Aersi Aierzhati[a], Michael J. Stablein[a], Niki E. Wu[b], Chih-Ting Kuo[c], Buchun Si[a], Xu Kang[a], Yuanhui Zhang[a,*]

[a] Department of Agricultural and Biological Engineering, University of Illinois at Urbana-Champaign, Champaign, IL, United States
[b] Department of Chemistry, University of Illinois at Urbana-Champaign, Champaign, IL, United States
[c] Illinois Sustainable Technology Center, University of Illinois at Urbana-Champaign, Champaign, IL, United States

GRAPHICAL ABSTRACT

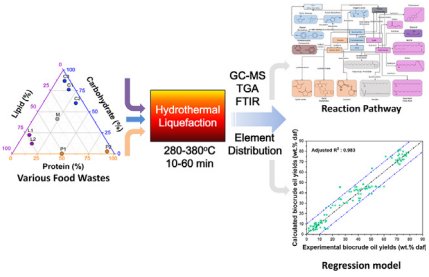

ARTICLE INFO

Keywords:
Food waste
Hydrothermal liquefaction
Elemental distribution
Reaction pathway
Predictive modeling

ABSTRACT

Excessive food waste presents an opportunity to simultaneously alleviate waste and produce renewable resources. The present work uses hydrothermal liquefaction (HTL) with elevated temperatures (280–380 °C) and times (10–60 min) to convert categorized food residues collected from a university campus dining hall into biocrude oil. Analysis of distinct feedstocks presented different biochemical compositions (protein, carbohydrate, and lipid) and yielded between 2 and 79% biocrude oil for the respective optimized HTL temperatures and times. Reaction pathways and elemental distributions (C,H,N) elucidated HTL product qualities based on feedstocks and optimized reaction conditions. Both descriptive HTL process energy recoveries and consumption ratios are included. An improved predictive model was able to accurately determine biocrude oil yield (R^2_{adj} 98.3%) of different food wastes under different reaction conditions, as well as predict previously published data (R^2 94.3%). Combined experimental and analytical results were used to assess the sustainability and robustness of the HTL process.

1. Introduction

Approximately one-third of food produced globally for human consumption is either lost or wasted (FAO, 2014) and about 60.7 million wet tons (assuming 75% moisture) of food waste was generated in the US (Skaggs et al., 2018). Natural decomposition of food wastes in landfills produces greenhouse gases, such as methane and CO_2, as well as leachate that contaminates surrounding soil and water (Vigano et al.,

* Corresponding author.
E-mail address: yzhang1@illinois.edu (Y. Zhang).

https://doi.org/10.1016/j.biortech.2019.03.076
Received 26 December 2018; Received in revised form 13 March 2019; Accepted 14 March 2019
Available online 16 March 2019
0960-8524/

2015). Many of these organic carbon and valuable nutrient rich residues are currently underutilized, however, there is potential value to be recuperated via an energy or resource recovery system. As such, several technologies have been implored for the sustainable processing of food waste, including incineration, pyrolysis, gasification, hydrothermal carbonization, fermentation, and anaerobic digestion (Thi Phuong Thuy et al., 2015). Thus, with the significant environmental benefit and energy recovery value, the conversion of food waste into biocrude oil, which can be used as renewable diesel blendstocks (Chen et al., 2018), is proposed in this study.

Hydrothermal liquefaction (HTL) is a technology that utilizes elevated temperatures and pressure near and below the critical point of water (374.2 °C and 22.1 MPa) to convert diverse wet biomasses (Dimitriadis and Bezergianni, 2017) into biocrude oil. This potentiates greater sustainability by simultaneously remediating the food waste going to landfills and producing renewable energy. The hydrothermal liquefaction process has been widely used in temperature ranging from 280 °C to 380 °C and residence time ranging from 10 to 90 min for various feedstocks (Xue et al., 2016). Hydrothermal processes have demonstrated fast conversion of biomass feedstocks into bio-crude oils, which are suitable for upgrading to liquid fuels (Xiu and Shahbazi, 2012). Additionally, HTL generates solid residues and nutrient dense aqueous coproducts that could be applied as fertilizers (Snowden-Swan et al., 2017; Lu et al., 2018a). Chemical interactions of HTL of microalgae, macroalgae, lignocellulosic biomass, and different model compounds were previously studied in detail (Changi et al., 2015; Deniel et al., 2016, 2017b; Madsen et al., 2017). However, information regarding the effects of reaction conditions on biocrude oil yield of real food waste and chemical interactions between their biochemical components is still limited. This work focused specifically on the impact of different reaction conditions and biochemical composition, which generate valuable results for future implementation of the technology.

Regression modeling has helped to predict oil yield and explain these complex reaction dynamics through the influence of different parameters. Previously published models (Biller and Ross, 2011; Leow et al., 2015; Li et al., 2017) have sought to estimate biocrude yield by linear summation of the yields obtained from HTL of individual model lipid, protein, and carbohydrate compounds and different types of microalgae. However, most models omit the effect of interactions between compounds, as well as operating conditions, on the biocrude yield. Teri et al. (2014), Lu et al. (2018b), and Sheng et al. (2018) proposed that these interactions influence the biocrude yield by using mixtures of different model compounds, but the effects of operating conditions were not included in the regression model. Yang et al. (2019) contributed a similar model with model compounds that considered time and temperature, using single, double, and triple variables in a single term, however, square terms of individual variables were not considered. Few studies have investigated modeling of hydrothermal liquefaction biocrude oil yield of real food waste. Deniel et al. (2017a) built a regression model with binary interaction terms for food processing residues under the same operating condition. After analysis of the experimental results with different feedstocks and reactor conditions, a model that more appropriately evaluates the effect of temperature, time, and feedstock composition, which is more accurate and complete for food waste, is needed.

In this study, a detailed hydrothermal liquefaction process of food waste was investigated. Food waste was separated into groups to represent the major biochemical categories and different qualities of food. This served to determine if particular food waste components were more ideal for HTL and production of biocrude oil products in terms of oil yield and quality, and energy balance reaction pathways for food waste HTL were also determined to better understand complex dynamics of product formation. An elemental analysis of the total products, which also include an aqueous phase and solids, also evaluated nutrient distribution for possible recovery. An improved regression modeling method based on food waste biochemical composition and reaction conditions using the present experimental data was developed, as well as being validated by previously published results. The conclusions from this research will improve food waste conversion via HTL, as well as generate an enhanced model that better predicts HTL yield for different feedstocks and operating conditions.

2. Materials and methods

2.1. Feedstock

The feedstocks used for HTL reactions in this study was a food waste mixture (M) collected from the University of Illinois at Urbana Champaign dining hall (Champaign, IL). Due to the varying effects on HTL yields that are influenced by protein, carbohydrate, and lipid content, the selection of traditional food waste subcomponents is very important. These subcomponents included are categorized in three groups and represented in the text with the following acronyms: high lipid group: salad dressing (L1), cream cheese (L2); high protein group: beef (P1), chicken (P2); high carbohydrate group: hamburger bun (C1), vegetable (C2), and fruit peels (C3). The salad dressing was a generic brand ranch. The vegetable feedstock was a mixture of tomato, carrot, and broccoli in a 1:1:1 wt ratio. Fruit peel was a 1:1 wt ratio mixture of orange peel and banana peel. The dry ash free weight percentages of lipid, protein, and carbohydrate content are presented in Fig. 1. The moisture content, ash content, CHN analysis, and higher heating value (HHV) of solid ingredients used as feedstocks are included in Table 1. Lignin is not included because, after testing, all the feedstocks had less than 0.5% lignin. The samples were stored at 4 °C upon preparation for experiments. Deionized water was used as the reaction medium for all experiments to achieve the predetermined moisture content. All other chemicals (≥99% purity) in this study were purchased from Sigma Aldrich. Ash content was measured according to ASTM E1755-01 method.

2.2. Hydrothermal liquefaction experiment

The 20 wt% feed solutions were hydrothermally treated at 280 °C, 300 °C, 320 °C, 340 °C, and 360 °C for 10–60 min in stainless steel cylinder batch reactors with a pressure range from 1.2 MPa to 11.0 MPa. Additionally, reactions at 380 °C were performed for two of the feedstocks. The volume of the reactor was 30.0 mL. 10 mL of feed solution was loaded. A high-pressure valve was attached to regulate pressure and collect the final gas product. Once the reactor was loaded and assembled, it was sealed and purged with nitrogen gas three times to displace headspace gases and set to an initial pressure of 0.5 MPa.

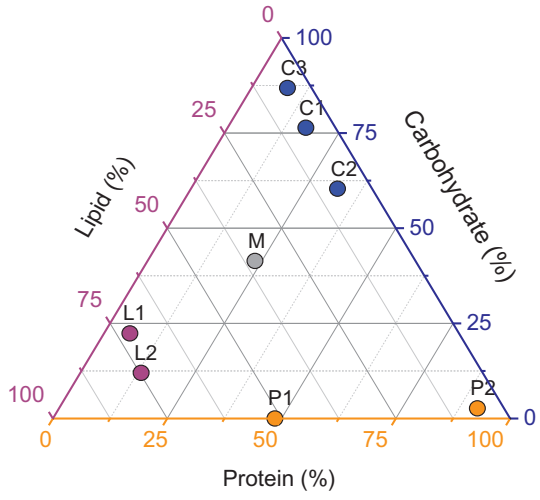

Fig. 1. Biochemical components on a dry ash free base of different feedstocks.

Table 1
Characterization of the feedstock that includes elemental analysis and higher heating value.

	Moisture content %	Ash content %	%				HHV (MJ·Kg^{-1})
			C	H	N	O*	
M	70.13 ± 0.05	4.68 ± 0.04	56.16 ± 1.27	8.05 ± 0.16	2.61 ± 0.19	33.19 ± 0.92	24.51 ± 0.33
L1	59.07 ± 0.03	4.89 ± 0.03	65.62 ± 0.54	9.99 ± 0.02	0.98 ± 0.02	23.41 ± 0.54	30.76 ± 0.50
L2	55.38 ± 0.02	3.10 ± 0.04	65.49 ± 0.11	10.19 ± 0.03	1.49 ± 0.06	22.84 ± 0.14	31.16 ± 0.05
P1	67.53 ± 0.01	2.30 ± 0.01	61.32 ± 0.02	9.29 ± 0.05	6.16 ± 0.55	23.24 ± 0.52	29.31 ± 0.40
P2	76.49 ± 0.01	4.68 ± 0.02	45.91 ± 0.23	6.91 ± 0.04	12.64 ± 0.33	34.55 ± 0.05	22.61 ± 0.87
C1	36.67 ± 0.05	2.37 ± 0.02	44.61 ± 0.05	6.44 ± 0.01	2.15 ± 0.08	46.81 ± 0.04	18.79 ± 0.01
C2	93.86 ± 0.04	13.11 ± 0.05	47.88 ± 3.19	7.03 ± 0.51	4.07 ± 0.04	41.03 ± 3.66	17.16 ± 0.05
C3	91.97 ± 0.04	5.00 ± 0.03	43.33 ± 0.47	5.75 ± 0.01	1.69 ± 0.01	49.25 ± 0.48	17.82 ± 0.03

*Oxygen is calculated by difference.

Electric resistance heating from a tube furnace (Thermo Scientific Lindberg Blue M) was used to keep the temperature at the desired condition. The reactor was put in when the furnace was at the desired reaction temperature. The reaction time began after heating for 3–4 min when the reactor surface reached the same temperature. For each of these feedstocks and conditions, the experiments were conducted in duplicate.

After the reaction was completed, the reactor was quenched with room temperature cooling water for 3 min to stop the reaction immediately. After cooling, the gas product was collected using a gas bag. It was analyzed by a gas chromatograph (Shimadzu Gas Chromatograph, GC-17A) with a TCD detector. The column was 18 ft long with an outer diameter of 1/8″ and packed with silica gel. The temperature of the column, detector, and injector was set to 140 °C, 150 °C, and 160 °C, respectively. In order to recover the oil product and residuals in the reactor, dichloromethane (DCM, CH_2Cl_2) was dispensed into the reactor. Then, the mixture went through a vacuum filter separation. Thus, both the liquid and solid phases were recovered separately. The solids obtained from the reactor were quantified using preweighted filter papers (Whatman No.4). The aqueous fraction and biocrude oil with dichloromethane (DCM) solvent were isolated in a separatory funnel through phase separation. The biocrude oil and aqueous phase were recovered separately afterward. Biocrude oil was collected after evaporating the dichloromethane (DCM) solvent and quantified by weight.

2.3. Elemental analysis

The C, H, and N contents of the HTL products (both oil and solid phases) were measured using a CE440 elemental analyzer (Exeter Analytical, North Chelmsford, MA). Oxygen contents were calculated by the difference subtracted from 100%. The aqueous phase was further analyzed for total carbon (TC) using a total organic carbon (TOC-VCPN) system with auto-sampler (Shimadzu Corporation, Kyoto, Japan), and total phosphorous (TP) using an ICP-OES system (PerkinElmer optima 8300). Total nitrogen (TN) of the aqueous phases was measured by using the Persulfate digestion method of HACH kits method 10072 (Rice et al., 2012).

2.4. Energy recovery calculation

The higher heating values (HHV, MJ·kg^{-1}) of feedstocks were measured using a Parr 6200 bomb calorimeter (Parr Instruments Company). HHV of the biocrude oil was estimated using the modified Dulong's formula (Chen et al., 2014) as given in Eq. (1).

$$\mathrm{HHV} = 0.0338 \times \mathrm{C} + 1.428\left(\mathrm{H} - \frac{\mathrm{O}}{8}\right) \quad (1)$$

where HHV is higher heating value (MJ·kg^{-1}), and C, H, and O are the mass percentage of carbon, hydrogen, and oxygen (%, w/w), respectively.

The oil yield was defined as the total mass of the oil phase relative to the total dry volatile organic compounds of the feed and was, then, calculated with Eq. (2).

$$\mathrm{Y} = \frac{M_{product}}{M_{feed} \times C_{feed}} \times 100\% \quad (2)$$

where Y is the oil yield (%, w/w); $M_{product}$ is the mass (g) of oil product; M_{feed} is the mass (g) of volatile organic compounds of feedstock; C_{feed} is the solid concentration (%, w/w) of the feedstock.

The thermochemical conversion energy of the process and energy recovered by biocrude oil was compared by calculating the energy consumption ratio (ECR), while accounting for energy loss and heat recovery efficiency. ECR values were calculated according to Eq. (3) (Vardon et al, 2012):

$$ECR_{HTL} = \frac{[C_{pw} W_i + (1 - W_i) C_{pf}] \Delta T [1 - R_h]}{Y(HHV)(1 - W_i) R_c} \quad (3)$$

where W_i is the feedstock water content; ΔT is the temperature increase (assumed 25 °C as initial temperature); C_{pw} is the specific heats of water (4.18 kJ·kg^{-1}·K^{-1}); R_h and R_c are the efficiencies of heat recovery and combustion assumed to be 0.5 and 0.7, respectively; Y is the biocrude oil yield, and HHV (kJ·kg^{-1}) is the higher heating value of the biocrude oil; and C_{pf} is the specific heat of a dewatered feedstock (kJ·kg^{-1}), which is calculated as follow:

$$C_{pf} = 4.18(0.2X_{salt} + 0.34X_{carbohydate} + 0.37X_{protein} + 0.4X_{lipid}) \quad (4)$$

where X represents the mass fraction % of each of the component groups (Rahman, 2009)

2.5. Thermogravimetric analysis (TGA)

Thermogravimetric Analysis (TGA) was determined with a Cahn TherMax 500 TGA system, using a quartz crucible to carry the biocrude oil samples. Biocrude oil samples of approximately 30 to 50 mg were used. The oven temperature was raised from 25 to 650 °C at a heating rate of 10 °C·min^{-1}, while under a 22 mL·min^{-1} nitrogen flow.

2.6. Gas chromatography mass spectroscopy (GC–MS)

A 2 μL sample was injected in a split mode (10:1) into the GC–MS system consisting of an Agilent 6890 gas chromatograph, an Agilent 5973 mass selective detector, and an Agilent 7683B autosampler. Gas chromatography was performed on a 60 m ZB-5MS column with 0.32 mm nominal diameter and 0.25 μm film thickness, using an injection temperature of 250 °C and Mass Selective Detector transfer line at 250 °C. The oven temperature was initially set to 70 °C with a hold time of 2 min, then increased at 5C·min^{-1} until reaching 300 °C, and held constant for 5 min. The source temperature was 230 °C, electron ionization was set at 70 eV, and spectra were scanned from 30 to 800 *m/z*. Individual peaks were identified by matching fragmentation

patterns against a NIST (NIST08) database.

2.7. Fourier transform infrared spectroscopy (FTIR)

The functional groups in the biocrude oils were detected by using Fourier transform infrared spectroscopy (FTIR). All spectra were collected with a Thermo Nicolet Nexus 670 Fourier transform infrared spectrophotometer in transmission mode and atmospheric compensated, between wavelengths of 800 and 4000 cm^{-1}. Prior to spectra measurement, the equipment was calibrated as background scans were collected. The beam splitter was KBr. An IR source was used. All spectra were collected at 4 cm^{-1} resolution at an average of 64 scans.

2.8. Predictive model

In previous research, individual reactions of proteins, lipids, and carbohydrates were modeled as first-order variables, and their binary interactions were modeled as an improvement for modeling of second-order variables (Sheng et al., 2018). On the other hand, Kumar and Pant (2016) modeled the effect of temperature and time more appropriately using a second-order polynomial regression equation. In the present study, a more complete regression model elaborated on the effects of feedstock biochemical composition and reaction conditions in a second-order polynomial with backward elimination, as follows:

$$Y(wt\%) = a + \sum_{i=1}^{5} b_i X_i + \sum_{i=1}^{5} c_i X_i^2 + \sum \sum_{i<j=1}^{5} d_i X_i X_j \quad (5)$$

where, Y is the biocrude oil yield in weight percentage; X_1, X_2, and X_3 are the lipid, protein, and carbohydrate content in the feedstock, respectively; X_4 is the reaction temperature; and X_5 is the reaction retention time. Calibration of this model for predicting biocrude yield was performed by nonlinear regression of biomass composition parameters (i.e., lipid, protein, carbohydrate, temperature and time) against corresponding HTL biocrude yields, using R software. The standard errors of the parameters were all less than 0.05. The regression analysis included analysis of variance (ANOVA) and residuals. The coefficients with a p-value larger than 0.05 were eliminated.

3. Results and discussion

3.1. Effect of biochemical components and reaction conditions on biocrude oil yield

Fig. 2a presents the oil yields for different food waste feedstocks via HTL from 280 to 380 °C. The biocrude oil yield varied from around 2% to 79% under different time and temperature conditions. The best yield for the food waste mixture (M) was 46.9% at 360 °C for 40 min. Notably, lipid rich feedstocks, salad dressing (L1) and cream cheese (L2), presented the greatest oil yields of 78.1% and 74.9%, respectively, both in the 320 °C condition for 40 min. The oil yield of beef (P1) increased from 280 °C to 300 °C, however, it decreased when the temperature was higher, achieving an oil yield of only 25.9% at 360 °C. On the other hand, the oil yield of chicken (P2) continually increased with the temperature from 280 °C to 360 °C. At 380 °C, when reaching the supercritical point of water inside the reactor, the yield decreased, as the gasification effect began to degrade and gasify the oil products. The difference of P1 and P2 likely to be caused by the lipid content in P1. The interaction between lipid and protein, especially between fatty acid hydrolyzed from lipid and amines degraded from protein, formed amides in P1 at lower temperatures. According to Changi et al. (2012), amines from proteins tend to be formed at lower temperatures, which explains the high biocrude oil yield of P1 at lower temperatures. The majority of the biocrude oil from P2 is from the Maillard reaction, which prefers higher temperatures (Fan et al., 2018). For the carbohydrate rich feedstocks, including C1, C2, and C3, the oil yield was significantly lower than other feedstocks. It should be noted that a large amount of solid residue was produced by these carbohydrate rich feedstocks, which contained a greater portion of the carbon in the solid fraction instead of the liquid product. These high carbohydrate containing feedstocks are more suitable for hydrothermal carbonization than liquefaction (Wang et al., 2018; Cantero-Tubilla et al., 2018).

Fig. 2b presents the relationship between reaction time and biocrude oil yield at the predetermined optimal temperature for each feedstock. The biocrude oil yield from all the feedstocks presented a trend of first increasing with reaction time and, then, slightly decreasing after passing the optimal reaction time (40 min). At first, L1 presented the highest yield in the condition of 40 min at 320 °C, but when optimizing time after temperature, this feedstock already had a 72% biocrude oil yield within 10 min of HTL. P1 also produced a high biocrude oil yield, being about 57.0% at 40 min, however, it dropped significantly to 43.9% when the reaction time increased to 60 min. C1, C2, and C3 did not have a comparably high biocrude oil at any retention time. Overall, the trends indicated that the influence of biochemical composition of feedstocks on the biocrude oil yield is ranked as lipid > protein > carbohydrate, which is consistent with previous studies (Biller and Ross, 2011; Teri et al., 2014).

3.2. Effect of biochemical composition on energy balance

The CHN and HHV values for the biocrude oil resulting from each of

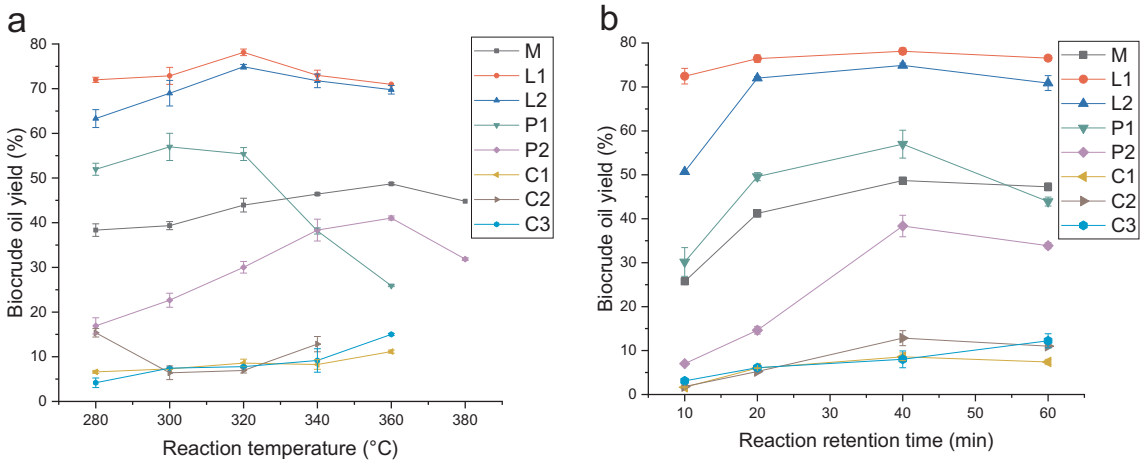

Fig. 2. a) Biocrude oil yield at different temperatures with 40 min reaction time; b) Biocrude oil yield at optimal temperature with different reaction times, M (360 °C), L1 (320 °C), L2 (340 °C), P1 (300 °C), P2 (360 °C), C1 (360 °C), C2 (360 °C), C3 (360 °C).

Table 2
Elemental analysis and higher heating value of the biocrude oils.

	%				HHV (MJ·Kg^{-1})
	C	H	N	O*	
M	74.37 ± 0.03	10.54 ± 0.03	3.52 ± 0.40	11.57 ± 0.46	38.15 ± 0.14
L1	75.22 ± 0.16	11.58 ± 0.08	0.31 ± 0.02	12.90 ± 0.26	39.68 ± 0.21
L2	74.99 ± 0.03	12.10 ± 0.16	0.23 ± 0.01	12.69 ± 0.19	40.38 ± 0.28
P1	73.61 ± 0.10	11.87 ± 0.10	1.68 ± 0.09	12.85 ± 0.28	39.56 ± 0.23
P2	67.99 ± 0.11	9.70 ± 0.03	8.68 ± 0.01	13.65 ± 0.09	34.41 ± 0.01
C1	73.71 ± 0.28	11.28 ± 0.04	1.11 ± 0.02	13.92 ± 0.29	38.55 ± 0.20
C2	69.64 ± 0.68	8.26 ± 0.14	6.07 ± 0.05	16.05 ± 0.86	32.48 ± 0.57
C3	72.78 ± 0.08	7.81 ± 0.03	2.28 ± 0.02	17.14 ± 0.06	32.71 ± 0.01

*Oxygen is calculated by difference.

Table 3
Process energy balance analysis of all feedstocks.

Feedstock	M	L1	L2	P1	P2	C1	C2	C3
ECR	0.23	0.12	0.13	0.16	0.31	1.31	1.04	0.88
Energy recovery (%)	72.2	95.8	94.0	75.1	59.5	17.2	21.0	26.2

the feedstocks at the ideal HTL operation condition are presented in Table 2. Among them, L1 and L2 had the highest energy recoveries of 95.8% and 94.0%, respectively. The food waste mixture (M) had an energy recovery of 73.1%. The energy recoveries from P1 and P2 were also notably high, although they were not as promising as the best values observed in this study. The energy recoveries from C1, C2, and C3 were relatively worse because of the lower oil yield and heating value. The energy consumption ratio (ECR) was calculated for the energy contained in the biocrude oil versus the energy required for thermochemical conversion. Despite C1 and C2 having an ECR greater than one, all other feedstocks had an ECR lower than one, which indicated that the food waste HTL process is net energy positive for most of the feedstocks in this study. Accordingly, the energy recovery and ECR of HTL were highly dependent on the feedstock biochemical compositions (Table 3).

3.3. Effect of biochemical composition on elemental distribution

The elemental distribution is an important indicator of the properties and further application of hydrothermal liquefaction products. Fig. 3 presents the distribution of carbon, nitrogen, and phosphorus for each of the resultant phases from the HTL of the various food waste feedstocks at the reaction conditions with highest biocrude oil yield. Several authors have reported the influence of feedstock composition and reaction conditions on the elemental composition of different HTL products (Zhu et al., 2017; Gollakota et al, 2018). For carbon distribution, L1 and L2 both have more than 80% of the carbon accumulated in the oil phase. It should be noted that this carbon accumulation is likely attributed to the high lipid content of the feedstocks. However, C1, C2, and C3 feedstocks also contain carbon but in the form of carbohydrates, which was seemingly transferred to the solid phase. Furthermore, the expectedly high cellulosic content of C2 and C3 will result in additional carbon transfer to the solid byproduct of HTL, which is formed from the fibers prior to dissolution (Barnes et al., 2017). P2, among the feedstocks, presented the greatest amount of carbon in the aqueous phase, which may result from the migration of carbon in nitrogenous compounds and short chain acids that are derived from protein degradation, and this conclusion was corroborated by the same effect seen in the P1 results. Carbohydrate degradation also resulted in carbon transfer to the aqueous phase by the formation of short chain organic acids. Other studies have also reported a significant portion of the carbon transferring to the aqueous phase (Bauer et al., 2018). Lastly, the feedstocks that had higher carbohydrate content and the

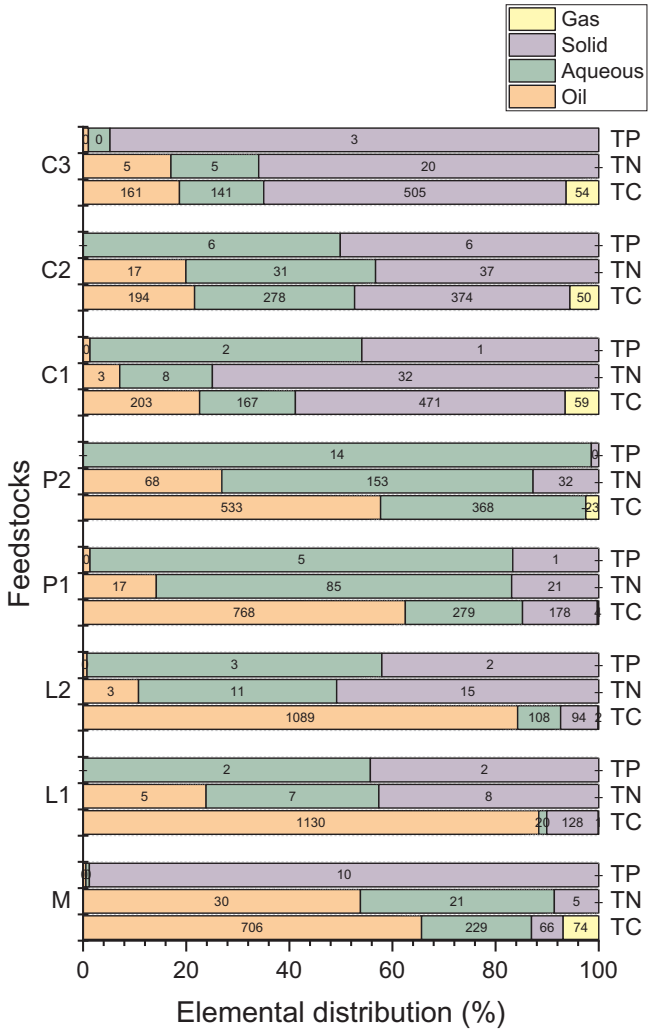

Fig. 3. Total carbon, nitrogen, and phosphorus distribution of biocrude oils from different feedstocks in each four phases, reaction temperatures are M (360 °C), L1 (320 °C), L2 (340 °C), P1 (300 °C), P2 (360 °C), C1 (360 °C), C2 (360 °C), C3 (360 °C) respectively, reaction time is 40 min. The numbers on the bars are the actual weight of the product based on mass balance in mg.

optimized conditions that used the highest temperatures resulted in some carbon transferring to the gas phase. Overall, there was notable variability in the carbon distribution observed among these HTL feedstocks.

Fig. 3 also presents the distribution of nitrogen to each of the resultant phases from the HTL of the various food waste feedstocks. For the food waste mixture, the interactions of the different food waste

components during HTL produced fatty acid amides and N-heterocyclic compounds as discussed in the next section and, thus, greater migration of nitrogen to the oil phase. P1 and P2 presented the highest total nitrogen content among all the feedstocks. For these high protein feedstocks, most of the nitrogen migrated to the aqueous phase in the form of ammonia. This high nitrogen content in the aqueous phase was also reported by Yu et al. (2011) when performing HTL on low-lipid algae. The decarboxylation reactions produced carbonic acid and amines, and deamination reactions produced ammonia and organic acids, as also observed by Posmanik et al. (2017). All these nitrogen containing organics are water soluble. These differences demonstrated that the distribution of nitrogen is highly dependent on the ratio of different biochemical components. Further analysis of the reaction pathway is needed for better understanding of the nitrogen distribution. Overall, the more complex matrix of the total food waste, thus, could dictate the variable distribution of the nitrogenous compounds, while the individual food waste components elucidate a clearer path for elemental distribution between the HTL products.

The distribution of the phosphorus in the various products is also shown by Fig. 3. These total phosphorous distribution results indicated that almost all of the phosphorus of M and C3 migrated to the solid residue. These particular retentions of the phosphorus suggest a means by which this element could be fractionated to the solids by binding with metals predominant in this phase, such as Ca and Mg (Jiang and Savage, 2018). Contrasting these results, L1, L2, C1, and C2 had only about 40–50% of the phosphorus in the solid residue, as it appeared to be evenly divided between the aqueous and solid residue. For other feedstocks, P1 and P2, most of the phosphorus was identified in the aqueous phase, likely because of metals in the aqueous phase that form precipitates with phosphorus (Yu et al., 2014), and the amount of solid residue generated by these two feedstocks was negligible. There was very little phosphorus quantified in the oil phase for any of the feedstocks. Further investigation on the binding of phosphorus to metals and its migration to different HTL products could explain how to achieve better recovery of this element for subsequent processes like algal growth, in addition to improving the quality of the biocrude.

3.4. Effect of biochemical composition on biocrude oil properties and reaction pathway

Fig. 4 summarizes the compounds with at least 0.5% relative peak area from the GC–MS tests of different feedstocks at the reaction conditions with highest biocrude oil yield. Biocrude oil is categorized as a mixture of long chain organic acids (saturated fatty acid, monounsaturated Fats (MUFAs), polyunsaturated Fats (PUFA)), amides and esters, hydrocarbons, N-heterocycle compounds, phenol derivatives and others. As can be seen in Fig. 4, the most detected compounds in the biocrude oil from feedstock M were MUFAs (*cis*-vaccenic acid, oleic acid and *cis*-9-hexadecenoic acid), saturated fatty acids (hexadecanoic acid, octadecanoic acid and tetradecanoic acid), and PUFAs (9,12-octadecadienoic acid (Z,Z)-), which were hydrolyzed from triacylglycerides (TAGs) and hydrogenated by sub-critical water (Vardon et al., 2011). The biocrude oil from L1 and L2 also contained these previously mentioned saturated fatty acid compounds but with different distributions. L1 was dominated by octadecanoic acid, however, L2 was dominated by hexadecanoic acid. In L1, four different types of C_{18} MUFAs (*cis*-vaccenic acid, *cis*-13-octadecenoic acid, *trans*-13-octadecenoic acid, and oleic Acid) were present. However, MUFAs and PUFAs in L2 were not present except for a small amount of *cis*-vaccenic acid. Additionally, monoglycerides were largely present in the L1 biocrude oil, which is the intermediate for TAGs. In the biocrude oil from high protein feedstocks (P1 and P2), fatty acid amides were present in a high percentage, which was likely the result of recombination between fatty acids and amines from protein degradation (Changi et al., 2015). Hexadecanamide, 9-octadecenamide, (Z)-, and octadecanamide were present in biocrude oil from P1. Hexadecanamide was the main fatty

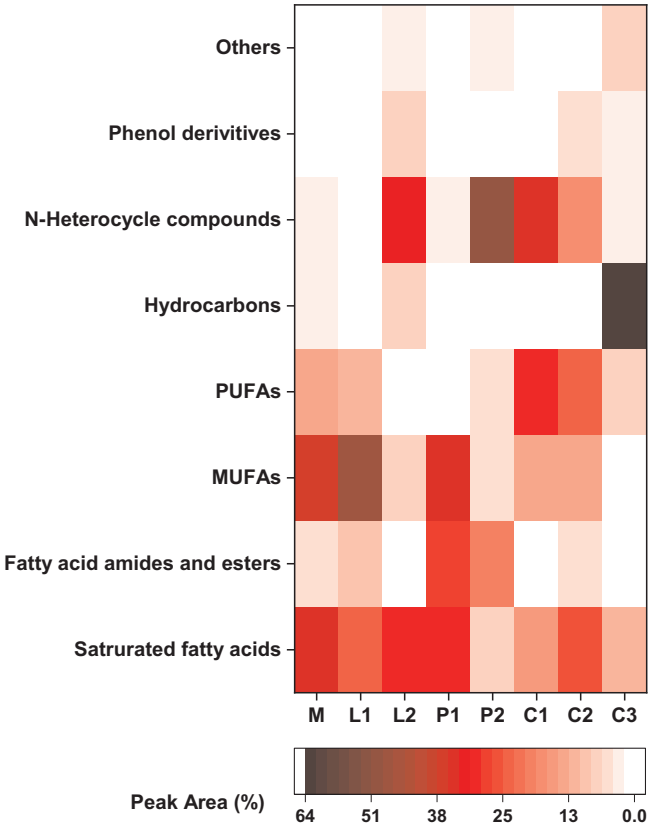

Fig. 4. Relative peak area percentage based on qualitative analysis by GC–MS of biocrude oils from different feedstocks, reaction temperatures are M (360 °C), L1 (320 °C), L2 (340 °C), P1 (300 °C), P2 (360 °C), C1 (360 °C), C2 (360 °C), C3 (360 °C) respectively, reaction time is 40 min.

acid amides in P2, however, it also contained four other type of fatty acid amides (C_6, C_{13}, C_{20}, C_{22}). Fatty acid, pyrrolidides were formed by a cyclization reaction of the amino acid (Fan et al., 2018). With a majority percentage of protein in the feedstock, a large amount of nitrogen heterocycles was detected in P2. Cyclo-Phe-Pro-diketopiperazine and Cyclo-Leu-Pro-diketopiperazine were the most present N-heterocyclic compounds, which were formed by cyclodehydration of amino acids with nonpolar R-groups (Changi et al., 2015). It should be noted that this type of reaction was observed for most feedstocks, as each contained at least some protein. However, diketopiperazines was further degraded at high temperature (Madsen et al., 2017), less of them were detected at M, C2, C3. Lactams from amino acid internal lactamization were also detected, as also observed by Fan et al. (2018). In P2, there were pyrroles, pyrazines, pyridines, and piperidines formed by the complex mechanism known as the Maillard reaction, which produces nitrogen heterocycles and nitrogenous polymers known as melanoidins (Peterson et al., 2010). These compounds were not present in P1 biocrude oil because of the lack of carbohydrate in feedstock. Products from amino acids cyclodehydration were detected in P1 as well. A small amount of cholesterol was also identified in all the above-mentioned samples (Brown et al., 2010). In the carbohydrate dominated feedstock, fatty acids were also present as the little amount of the lipid in feedstock. However, C3 presented a high percentage of benzene derivatives and cyclic ketones, which is believed to be products of aldol splitting, cyclization, and rearrangement of carbohydrates (Changi et al., 2015). C1 and C2 presented greater amounts of N-heterocycle than C3, which indicated that protein component was essential for forming the N-heterocycle compounds. Further research is needed on the complex Maillard reactions network. A detailed reaction pathway of food waste HTL based on the GC–MS analysis of this study, as well as

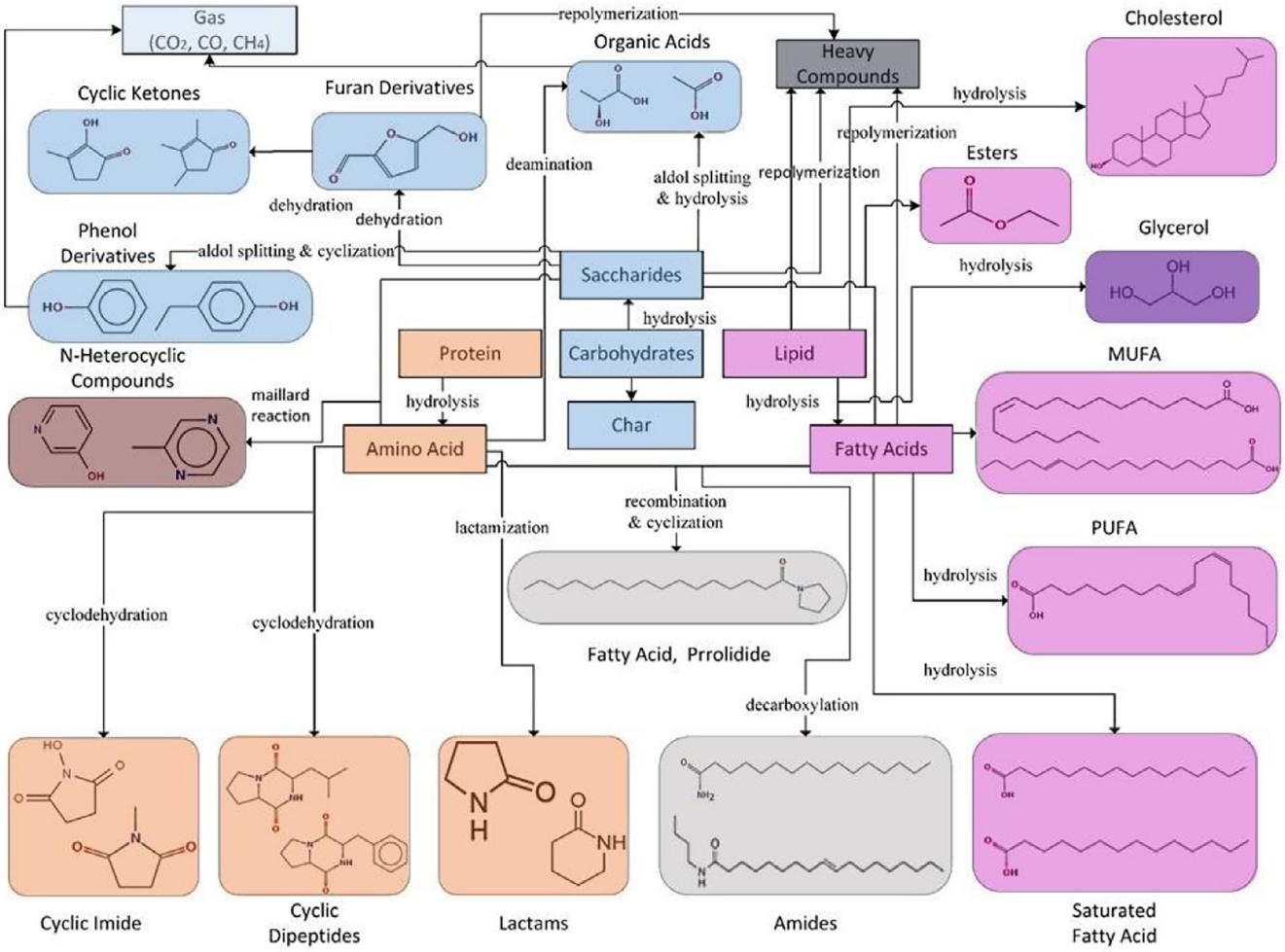

Fig. 5. Food waste HTL reaction network with different colors representing the identified compounds from lipid, protein, carbohydrate or their interactions. The potential conversion reactions were also marked on the connection lines.

previous published suggestions, can be seen in Fig. 5. One or two compounds with the largest peak areas were picked to represent each category. The results presented here can now be used to improve the understanding of reaction mechanisms for food waste hydrothermal liquefaction.

Hydrothermal liquefaction biocrude contains a wide range of oils, including both lower boiling point compounds that are ideal for fuel and higher boiling point chemicals that can serve as lubricants and asphalt binders. GC–MS results can only quantify compounds with a boiling point lower than 300 °C, which is considered to be in the range of gasoline, jet fuel, and diesel. This study presented the results for the thermogravimetric analysis (TGA) and differential thermogravimetry (DTG) of the biocrude oils in Supplementary material, which provides a comprehensive evaluation of its thermal properties. Majority of the weight loss of feedstocks M, P2, C1, C2, and C3 were in the kerosene (149–232 °C) and gas oil range (232–343 °C), according to the classification for petroleum products (Speight, 2002). However, the biocrude oil from L1, L2, and P1 had a significant weight change in the heavy vacuum gas oil range (371–566 °C), which is outside the detection range of GC–MS. This indicated that although high lipid content lead to high biocrude oil yield, the biocrude oil from high lipid feedstocks had a significantly large portion of heavy oil which only thermally degraded above 350 °C because of pyrolysis. These compounds are considered to be of high heteroatom content, for instance dimers and polyaromatics, that were formed by the recombination effect of fatty acids, which indicates the need for biocrude oil upgrading to convert this product to a transportation fuel substitute. Finally, it was determined that the end of the biocrude oil distillation (or evaporation behavior) occurred around 500 °C, where there was no significant weight change after this point.

The FTIR spectra for the different biocrude oil products from the different food waste feedstocks used in this study can be seen in the Supplementary material. All the biocrude oil samples, regardless of the feedstocks type, showed prominent peaks at 2850–2960 cm^{-1}, indicating the presence of C–H stretching from alkyl groups. The peak at 1708 cm^{-1} indicated C═O stretching vibration from carboxylic groups, which indicated ketones and aldehydes (Singh et al., 2015). The C–H bending vibration at 1370 cm^{-1} from alkyl groups and the CH_2 bending vibration at 1460 cm^{-1} from alkylated compounds with the C-O bending vibration at 1215 cm^{-1}, especially in L1, L2, and P1, suggested the presence of fats and esters (Zou et al., 2009), which is consistent with the GC–MS results. Additionally, according to Huang et al. (2016), peaks at 1150–1730 cm^{-1} indicated the presence of N and O heteroatoms, which reflected the same results from the elemental analysis and GC–MS test. FTIR is a useful tool that can help to identify specific bonds in HTL products, as a complement to the GC–MS test.

3.5. Prediction model based on the biochemical composition and reaction conditions

Linear prediction models began by considering the HTL of a feedstock mixture as the linear combination of the HTL results from pure components (Biller and Ross, 2011). The cross-interaction significantly

affects the biocrude yield and the accuracy of the linear summation model, which has since been investigated by many researchers (Leow et al., 2015; Li et al., 2017; Teri et al., 2014; Sheng et al, 2018). However, previous researches established models for certain reaction condition and mostly focused on microalgae, which did not present a high accuracy in prediction of food waste biocrude oil yield when comparing with the experimental results of this study, as shown in Supplementary material.

For the experiments conducted in this research, a model considering both feedstock components and reaction conditions was calibrated. Bayesian information criterion (BIC) was performed for model selection of 20 different parameter combinations in Eq. (5). It was determined that 9 variables presented the lowest BIC, which was the final number of variables in the model. The best subset was picked by using all selected variables that had statistically significant impact on biocrude oil yield and highest regression R^2 for the model. This research evaluated different biochemical composition from food waste and provides a complete prediction model for the HTL processes of different biochemical compositions, resulting in a second order polynomial presented as equation (6).

$$Y\,(wt\%) = 1.61X_l - 0.558X_p - 0.00625T_r^2 + 0.00565X_p^2 + 0.00324T_R T_r + 0.0108X_l X_c - 0.00273X_l T_R - 0.00465X_l T_r - 0.00772X_c T_r \quad (6)$$

where, Y is the biocrude oil yield in weight percentage; X_l, X_p, and X_c are the lipid, protein, and carbohydrate content (wt.%) in the feedstock dry weight, respectively; T_R is the reaction temperature (°C); and T_r is the reaction retention time (min).

As shown in Fig. 6a, the dataset collected in this study presented an R^2 value of 0.983. As noted by the large, positive coefficient value, the percentage of lipids in the feedstock contributes the most to the final oil yield, as also reported in previous studies (Leow et al., 2015; Teri et al., 2014; Sheng et al, 2018). As described in Section 3.4, protein content was also a significant factor for the oil yield. There was no significant effect of carbohydrate content on the biocrude oil, and thus, this factor was eliminated. The interaction of lipid and carbohydrate contributed positively to the oil yield, which was also observed in the GC–MS results discussed in section 3.4. The coupling effect of temperature and time with lipid and carbohydrate together affect the biocrude oil yield. Reaction temperature and time are essential for the accuracy of predicting biocrude oil yield.

This model also successfully predicted the data from other relatively limited numbers of studies on real food waste HTL studies that reported biochemical composition information. In order to test the potential for broader application of this model, several algal HTL studies with either similar reactor type or similar product recovery method were selected with consideration for different reaction conditions. As presented in Fig. 6b, the present model predicted these biocrude oil yields at an R^2 of 0.943. Prediction of the food waste HTL biocrude oil yield was the primary goal of this model. Because the nature of the feedstock has other qualities that are not included in the range of study for the present model, prediction of algal HTL biocrude oil is not as good as food waste. In other words, this model is not a general biocrude oil yield prediction model for hydrothermal liquefaction of biomass because of the limitation on the scope of this research. Many other variables that can affect the biocrude oil yield, for example, heating rate, reactor type, solid content of feedstock, and the difference of biochemical compositions on a molecular level between different feedstocks were not considered. However, this model was an improvement from previous iterations on food waste HTL and a demonstration of a successful combination of statistical analysis methods with biomass prediction models. The prediction modeling method established in this study can be further developed to include other parameters, when the experimental data is available, for potential broader applications.

4. Conclusions

Raw food waste from a campus dining hall presented a promising biocrude oil yield via hydrothermal liquefaction. The results indicated that the biochemical composition of food waste had a significant effect on both the oil yield and various product composition and properties. The distribution of elements and reaction mechanisms were highly dependent on the feedstock biochemical composition. An improved regression model, considering both biochemical composition and reaction conditions, was developed. This study provides a significant basis for food waste HTL by providing in depth analysis to improve energy and nutrient recovery, which has increasing global demand and application.

Acknowledgments

The authors would like to acknowledge financial support from the University of Illinois at Urbana Champaign Student Sustainable Committee (SSC), and the National Science Foundation (NSF CBET 17-44775).

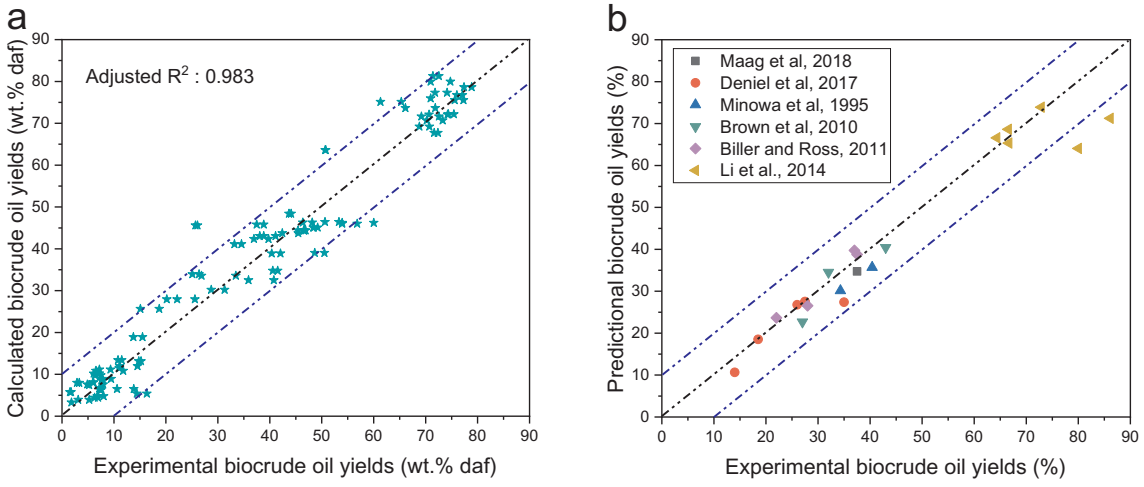

Fig. 6. Comparison of biocude oil yield obtained by the model of this study. a) Parity plot of calculated biocude oil yield and data collected in this study; b) Parity plot of predictions with other published studies.

Appendix A. Supplementary data

Supplementary data to this article can be found online at https://doi.org/10.1016/j.biortech.2019.03.076.

References

Barnes, M.C., Oltvoort, J., Kersten, S.R.A., Lange, J.-P., 2017. Wood liquefaction: role of solvent. Ind. Eng. Chem. Res. 56 (3), 635–644.

Bauer, S.K., Reynolds, C.F., Peng, S., Colosi, L.M., 2018. Evaluating the water quality impacts of hydrothermal liquefaction assessment of carbon, nitrogen, and energy recovery. Bioresour. Technol. Rep. 2, 115–120.

Biller, P., Ross, A.B., 2011. Potential yields and properties of oil from the hydrothermal liquefaction of microalgae with different biochemical content. Bioresour. Technol. 102 (1), 215–225.

Brown, T.M., Duan, P.G., Savage, P.E., 2010. Hydrothermal Liquefaction and gasification of nannochloropsis sp. Energy Fuels 24 (6), 3639–3646.

Cantero-Tubilla, B., Cantero, D.A., Martinez, C.M., Tester, J.W., Walker, L.P., Posmanik, R., 2018. Characterization of the solid products from hydrothermal liquefaction of waste feedstocks from food and agricultural industries. J. Supercrit. Fluids 133, 665–673.

Changi, S., Zhu, M., Savage, P.E., 2012. Hydrothermal reaction kinetics and pathways of phenylalanine alone and in binary mixtures. ChemSusChem 5 (9), 1743–1757.

Changi, S.M., Faeth, J.L., Mo, N., Savage, P.E., 2015. Hydrothermal reactions of biomolecules relevant for microalgae liquefaction. Ind. Eng. Chem. Res. 54 (47), 11733–11758.

Chen, W.-T., Zhang, Y., Zhang, J., Schideman, L., Yu, G., Zhang, P., Minarick, M., 2014. Co-liquefaction of swine manure and mixed-culture algal biomass from a wastewater treatment system to produce bio-crude oil. Appl. Energy 128, 209–216.

Chen, W.-T., Zhang, Y., Lee, T.H., Wu, Z., Si, B., Lee, C.-F.F., Lin, A., Sharma, B.K., 2018. Renewable diesel blendstocks produced by hydrothermal liquefaction of wet biowaste. Nature Sust. 1 (11), 702–710.

Deniel, M., Haarlemmer, G., Roubaud, A., Weiss-Hortala, E., Fages, J., 2016. Energy valorisation of food processing residues and model compounds by hydrothermal liquefaction. Renew. Sustain. Energy Rev. 54, 1632–1652.

Deniel, M., Haarlemmer, G., Roubaud, A., Weiss-Hortala, E., Fages, J., 2017a. Modelling and predictive study of hydrothermal liquefaction: application to food processing residues. Waste Biomass Valorization 8 (6), 2087–2107.

Deniel, M., Haarlemmer, G., Roubaud, A., Weiss-Hortala, E., Fages, J., 2017b. Hydrothermal liquefaction of blackcurrant pomace and model molecules: understanding of reaction mechanisms. Sustain. Energy Fuels 1 (3), 555–582.

Dimitriadis, A., Bezergianni, S., 2017. Hydrothermal liquefaction of various biomass and waste feedstocks for biocrude production: a state of the art review. Renew. Sustain. Energy Rev. 68, 113–125.

Fan, Y., Hornung, U., Dahmen, N., Kruse, A., 2018. Hydrothermal liquefaction of protein-containing biomass: study of model compounds for Maillard reactions. Biomass Convers. Biorefin. 8 (4), 909–923.

FAO, 2014. Food Losses and Waste in the Context of Sustainable Food Systems—a report by the high level panel of experts on food security and nutrition. Available at: http://www.fao.org/3/a-i3901e.pdf.

Gollakota, A.R.K., Kawale, H.D., Kishore, N., Gu, S., 2018. A review on hydrothermal liquefaction of biomass (vol 81, pg 1378, 2018). Renew. Sustain. Energy Rev. 98, 515–517.

Huang, Y.Q., Chen, Y.P., Xie, J.J., Liu, H.C., Yin, X.L., Wu, C.Z., 2016. Bio-oil production from hydrothermal liquefaction of high-protein high-ash microalgae including wild Cyanobacteria sp and cultivated Bacillariophyta sp. Fuel 183 (9–19), 47.

Jiang, J., Savage, P.E., 2018. Metals and other elements in biocrude from fast and isothermal hydrothermal liquefaction of microalgae. Energy Fuels 32 (4), 4118–4126.

Kumar, D., Pant, K.K., 2016. Biorefinery solid cake waste to biocrude via hydrothermal treatment: optimization of process parameters using statistical approach. Biomass Convers. Biorefin. 6 (1), 79–90.

Leow, S., Witter, J.R., Vardon, D.R., Sharma, B.K., Guest, J.S., Strathmann, T.J., 2015. Prediction of microalgae hydrothermal liquefaction products from feedstock biochemical composition. Green Chem. 17 (6), 3584–3599.

Li, Y.L., Leow, S., Fedders, A.C., Sharma, B.K., Guest, J.S., Strathmann, T.J., 2017. Quantitative multiphase model for hydrothermal liquefaction of algal biomass. Green Chem. 19 (4), 1163–1174.

Lu, J., Li, H., Zhang, Y., Liu, Z., 2018a. Nitrogen migration and transformation during hydrothermal liquefaction of livestock manures. ACS Sustain. Chem. Eng. 6 (10), 13570–13578.

Lu, J., Liu, Z., Zhang, Y., Savage, P.E., 2018b. Synergistic and antagonistic interactions during hydrothermal liquefaction of soybean oil, soy protein, cellulose, xylose, and lignin. ACS Sustain. Chem. Eng. 6 (11), 14501–14509.

Madsen, R.B., Zhang, H., Biller, P., Goldstein, A.H., Glasius, M., 2017. Characterizing semivolatile organic compounds of biocrude from hydrothermal liquefaction of biomass. Energy Fuel 31 (4), 4122–4134.

Peterson, A.A., Lachance, R.P., Tester, J.W., 2010. Kinetic evidence of the maillard reaction in hydrothermal biomass processing: glucose-glycine interactions in high-temperature. High-Pressure Water. Ind. Eng. Chem. Res. 49 (5), 2107–2117.

Posmanik, R., Cantero, D.A., Malkani, A., Sills, D.L., Tester, J.W., 2017. Biomass conversion to bio-oil using sub-critical water: study of model compounds for food processing waste. J. Supercrit. Fluids 119, 26–35.

Rahman, M.S. (Ed.), 2009. Food Properties Handbook, second ed. CRC Press, New York, NY.

Rice, E.W., Baird, R.B., Eaton, A.D., Clesceri, L.S., 2012. Standard Methods for the examination of water and wastewater, 22nd ed. American Public Health Association, Washington, pp. 1360.

Sheng, L., Wang, X., Yang, X., 2018. Prediction model of biocrude yield and nitrogen heterocyclic compounds analysis by hydrothermal liquefaction of microalgae with model compounds. Bioresour. Technol. 247 (14–20), 46.

Singh, R., Bhaskar, T., Balagurumurthy, B., 2015. Effect of solvent on the hydrothermal liquefaction of macro algae Ulva fasciata. Process Saf. Environ. 93, 154–160.

Skaggs, R.L., Coleman, A.M., Seiple, T.E., Milbrandt, A.R., 2018. Waste-to-Energy biofuel production potential for selected feedstocks in the conterminous United States. Renew. Sustain. Energy Rev. 82, 2640–2651.

Snowden-Swan, L.J., Zhu, Y., Bearden, M.D., Seiple, T.E., Jones, S.B., Schmidt, A.J., Billing, J.M., Hallen, R.T., Hart, T.R., Liu, J., Albrecht, K.O., Fox, S.P., Maupin, G.D., Elliott, D.C., 2017. Conceptual Biorefinery Design and Research Targeted for 2022: Hydrothermal Liquefaction Processing of Wet Waste to Fuels. PNNL-27186, Richland, WA.

Speight, J.G., 2002. Handbook of Petroleum Product Analysis. A John Wiley & Sons, Inc, Hoboken, New Jersey.

Teri, G., Luo, L., Savage, P.E., 2014. Hydrothermal treatment of protein, polysaccharide, and lipids alone and in mixtures. Energy Fuels 28 (12), 7501–7509.

Thi Phuong Thuy, P., Kaushik, R., Parshetti, G.K., Mahmood, R., Balasubramanian, R., 2015. Food waste-to-energy conversion technologies: current status and future directions. Waste Manage. 38, 399–408.

Vardon, D.R., Sharma, B.K., Scott, J., Yu, G., Wang, Z.C., Schideman, L., Zhang, Y.H., Strathmann, T.J., 2011. Chemical properties of biocrude oil from the hydrothermal liquefaction of Spirulina algae, swine manure, and digested anaerobic sludge. Bioresour. Technol. 102 (17), 8295–8303.

Vardon, D.R., Sharma, B.K., Blazina, G.V., Rajagopalan, K., Strathmann, T.J., 2012. Thermochemical conversion of raw and defatted algal biomass via hydrothermal liquefaction and slow pyrolysis. Bioresour. Technol. 109, 178–187.

Vigano, J., da Fonseca Machado, A.P., Martinez, J., 2015. Sub- and supercritical fluid technology applied to food waste processing. J. Supercrit. Fluids 96, 272–286.

Wang, T., Zhai, Y., Li, H., Zhu, Y., Li, S., Peng, C., Wang, B., Wang, Z., Xi, Y., Wang, S., Li, C., 2018. Co-hydrothermal carbonization of food waste-woody biomass blend towards biofuel pellets production. Bioresour. Technol. 267, 371–377.

Xiu, S., Shahbazi, A., 2012. Bio-oil production and upgrading research: a review. Renew. Sustain. Energy Rev. 16 (7), 4406–4414.

Xue, Y., Chen, H., Zhao, W., Yang, C., Ma, P., Han, S., 2016. A review on the operating conditions of producing bio-oil from hydrothermal liquefaction of biomass. Int. J. Energy Res. 40 (7), 865–877.

Yang, J., He, Q., Corscadden, K., Niu, H., Lin, J., Astatkie, T., 2019. Advanced models for the prediction of product yield in hydrothermal liquefaction via a mixture design of biomass model components coupled with process variables. Appl. Energy 233–234, 906–915.

Yu, G., Zhang, Y., Schideman, L., Funk, T., Wang, Z., 2011. Distributions of carbon and nitrogen in the products from hydrothermal liquefaction of low-lipid microalgae. Energy Environ. Sci. 4 (11), 4587–4595.

Yu, G., Zhang, Y.H., Guo, B., Funk, T., Schideman, L., 2014. Nutrient flows and quality of bio-crude oil produced via catalytic hydrothermal liquefaction of low-lipid microalgae. Bioenergy Res. 7 (4), 1317–1328.

Zhu, Z., Si, B., Lu, J., Watson, J., Zhang, Y., Liu, Z., 2017. Elemental migration and characterization of products during hydrothermal liquefaction of cornstalk. Bioresour. Technol. 243, 9–16.

Zou, S.P., Wu, Y.L., Yang, M.D., Li, C., Tong, J.M., 2009. Thermochemical catalytic liquefaction of the marine microalgae dunaliella tertiolecta and characterization of bio-oils. Energy Fuels 23 (7), 3753–3758.